The Astrophysical Journal, 641:556–564, 2006 April 10

ANGULAR DIFFERENTIAL IMAGING: A POWERFUL HIGH-CONTRAST IMAGING TECHNIQUE[1]

Christian Marois,[2,3] David Lafrenière,[2] René Doyon,[2] Bruce Macintosh,[3] and Daniel Nadeau[2]

Received 2005 October 13; accepted 2005 December 9

ABSTRACT

Angular differential imaging is a high-contrast imaging technique that reduces quasistatic speckle noise and facilitates the detection of nearby companions. A sequence of images is acquired with an altitude/azimuth telescope while the instrument field derotator is switched off. This keeps the instrument and telescope optics aligned and allows the field of view to rotate with respect to the instrument. For each image, a reference point-spread function (PSF) is constructed from other appropriately selected images of the same sequence and subtracted to remove quasistatic PSF structure. All residual images are then rotated to align the field and are combined. Observed performances are reported for Gemini North data. It is shown that quasistatic PSF noise can be reduced by a factor $\sim$5 for each image subtraction. The combination of all residuals then provides an additional gain of the order of the square root of the total number of acquired images. A total speckle noise attenuation of 20–50 is obtained for a 1 hr long observing sequence compared to a single 30 s exposure. A PSF noise attenuation of 100 was achieved for a 2 hr long sequence of images of Vega, reaching a 5 σ contrast of 20 mag for separations greater than 8″. For a 30 minute long sequence, ADI achieves signal-to-noise ratios 30 times better than a classical observation technique. The ADI technique can be used with currently available instruments to search for $\sim 1 M_{\rm Jup}$ exoplanets with orbits of radii between 50 and 300 AU around nearby young stars. The possibility of combining the technique with other high-contrast imaging methods is briefly discussed.

Subject headings: instrumentation: adaptive optics — planetary systems — stars: imaging

1. INTRODUCTION

Direct detections of very faint exoplanets and brown dwarfs near bright stars are essential in understanding substellar formation and evolution around stars. This endeavor is now one of the major goals for next-generation 10 m telescope instruments and future 30 to 100 m telescopes. The task is dauntingly difficult. The exoplanet or brown dwarf image is usually much fainter than the background from the brilliant stellar point-spread function (PSF) image. Aside from the Poisson noise, ground-based telescopes suffer from atmospheric turbulence that produces random short-lived speckles that mask faint companions. If these two limitations were the only ones, a simple solution would be to integrate longer to average these random noises and gain as the square root of the integration time. However, observations have shown that for integrations longer than a few minutes, the PSF noise converges to a quasistatic noise pattern, thus preventing a gain with increasing integration time (Marois et al. 2003, 2005; Masciadri et al. 2005). To achieve better detection limits, it is thus necessary to subtract the quasistatic noise using a reference PSF. Both ground- and space-based imaging are plagued with this stellar PSF calibration problem caused by imperfect optics and slowly evolving optical alignments. For ground-based imaging, subtraction of a reference PSF obtained from a star close to the target achieves a factor $\sim$4 of PSF noise attenuation, leaving residuals that are also quasistatic and thus severely limiting detection of fainter companions (Marois et al. 2005). For space-based telescopes that have a better PSF stability, like the *Hubble Space Telescope* (*HST*), a partial solution was found by subtracting two stellar images acquired during the same orbit with a different roll angle. This technique, called "roll deconvolution," successfully subtracts the stellar image by a factor of 50 (Schneider & Silverstone 2003; Fraquelli et al. 2004), but is also ultimately limited by PSF evolution. A similar technique, called angular differential imaging (ADI), can be used on ground-based altitude/azimuth telescopes to subtract a significant fraction of the stellar quasistatic noise and can potentially achieve detection limits that improve as the square root of the integration time.

In this paper, the ADI technique is described and its performance is analyzed using a simple analytical model and data from the Gemini Altair adaptive optics system and the NIRI near-infrared camera. The PSF stability with Altair NIRI is studied, and its impact on ADI performances is discussed. Detection limits for three stars of our ongoing young nearby star survey are then shown. A comparison between ADI and normal imaging is also presented. Finally, the possibility of using ADI with other high-contrast imaging techniques is discussed.

2. THE ANGULAR DIFFERENTIAL IMAGING TECHNIQUE

ADI is a PSF calibration technique that can, in principle, suppress the PSF quasistatic structure by a large factor (Marois 2004). It consists of the acquisition of a sequence of images with an altitude/azimuth telescope and the instrument rotator turned off (at the Cassegrain focus) or adjusted (Nasmyth) to keep the instrument and telescope optics aligned. This setup improves the stability of the quasistatic PSF structure throughout the sequence, while it causes a slow rotation of the field of view (FOV) with respect to the instrument. Note that only the FOV, not the PSF, rotates with time. Since the FOV rotates during an exposure, companion PSFs are smeared azimuthally. This effect increases

[1] Based on observations obtained at the Gemini Observatory, which is operated by the Association of Universities for Research in Astronomy, Inc., under a cooperative agreement with the NSF on behalf of the Gemini partnership: the National Science Foundation (United States), the Particle Physics and Astronomy Research Council (United Kingdom), the National Research Council (Canada), CONICYT (Chile), the Australian Research Council (Australia), CNPq (Brazil), and CONICET (Argentina).

[2] Département de Physique and Observatoire du Mont Mégantic, Université de Montréal, C.P. 6128, Succ. A, Montréal, QC H3C 3J7, Canada; david@astro.umontreal.ca, doyon@astro.umontreal.ca, nadeau@astro.umontreal.ca.

[3] Institute of Geophysics and Planetary Physics L-413, Lawrence Livermore National Laboratory, 7000 East Ave, Livermore, CA 94550; cmarois@igpp.ucllnl.org, bmac@igpp.ucllnl.org.

linearly with angular separation and slightly decreases companions peak intensity. Short exposures and the use of an optimized aperture photometry box can minimize this effect. For each image, after data reduction and image registration of the whole sequence, a reference PSF obtained from other images of the same sequence is subtracted to remove the quasistatic structure. Given enough FOV rotation during the sequence, this subtraction preserves the signal from any eventual companion. All the image differences are then rotated to align the FOV and are median combined.

This technique offers a number of advantages over more classical ground-based observations, since the target observations themselves are used to construct a reference PSF. This means that the reference PSF has the same spectrum and brightness as the target and that no time is lost to acquiring reference observations of a different target. Ghost images from optical reflections and the sky flux are also removed by the subtraction. The detector flat-field errors are averaged, since the FOV is integrated with different pixels as it rotates on the detector. The ADI technique is a generalization of the "roll deconvolution" technique used with *HST* since several images, each at a different field angle, are acquired and combined. A technique similar to ADI has been developed independently by Liu (2004) to search for circumstellar disks.

3. NOISE ATTENUATION THEORY WITH ADI

For each reduced and registered image of an ADI sequence, a reference PSF must be built from the images of the same sequence. The way in which this reference PSF is built is of great importance, since it directly affects the noise attenuation performance. We have used two methods to construct the reference PSF.

The first method is simply to take the median of all the images of the sequence. If enough field rotation has occurred during the sequence so that an eventual point source has moved by at least twice its full width at half maximum (FWHM), then this point source will be largely rejected by the median, which will leave only the average PSF. The minimum radial separation at which this occurs is noted as $R_{\min}$. Since the median is taken over a large number of images, the pixel-to-pixel noise (i.e., PSF, flat field, dark and sky Poisson noises, and detector readout noise) of the reference image is much less than that of any individual image. Thus, this first method minimizes the noise in regions where the residuals are limited by pixel-to-pixel noise. However, since a sequence typically lasts more than an hour, the reference PSF only has modest quasistatic speckle correlation with the individual images of the sequence.

The second method is to take the median of only a few images as close in time as possible, but for which the displacement due to field rotation between the images is, at a given separation, at least 1.5 PSF FWHM. This displacement ensures that the flux inside the PSF core of an eventual point source is not significantly reduced by the subtraction. The time $\tau_{\min}$ required for such field rotation is function of the separation angle from the target, the target azimuth A, zenith distance z, and the telescope latitude ϕ. The rotation rate ψ (degrees per minute) of the FOV is obtained from the time derivative of the parallactic angle and is given (McLean 1997, chap. 3) by

$$\psi = 0.2506 \frac{\cos A \cos \phi}{\sin z}. \tag{1}$$

Figure 1 is provided as a reference to determine the time interval for observations from the summit of the Mauna Kea. This second technique provides better quasistatic speckle noise attenuation, since the reference PSF is built using images acquired at short time

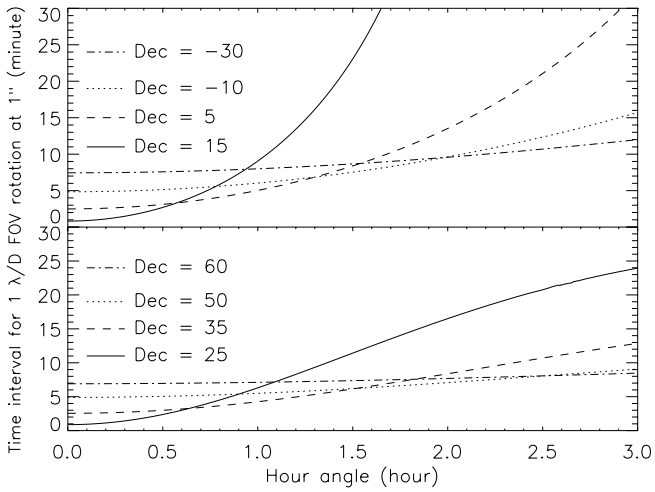

FIG. 1.—Interval of time required for a point source to move by 1 λ/D (1.6 μm on an 8 m diameter telescope) at 1″ as a function of hour angle for various declinations. Calculated for Mauna Kea, Hawaii.

intervals. However, the pixel-to-pixel noise of the reference image may not be negligible compared to that of an individual image.

The first method is optimized for regions where the residuals are limited by pixel-to-pixel noise, while the second is optimized for regions where the residuals are still limited by speckle noise. The combination of both techniques into a single reduction algorithm is discussed in § 5.2.

The ADI technique attenuates the PSF noise in two steps, (1) by subtraction of a reference image to remove correlated speckles and (2) by the combination of all residual images after FOV alignment to average the residual noise. The noise attenuation $N/\Delta N$ is defined as the ratio of the local noise N in an image over the noise ΔN of the residual image.

The noise attenuation obtained by the subtraction of the reference PSF, $[N/\Delta N]_S(\theta, \tau, t_{\exp})$, is a function of the angular separation θ, the time interval τ between the image and its reference, and the individual image exposure time $t_{\exp}$ (including overheads). Strong quasistatic speckle correlation between successive images leads to strong attenuation and thus better detection limits for a given total integration time. A good and stable seeing is thus expected to deliver better ADI quasistatic speckle attenuation. For a perfect case when all static and quasistatic speckles have been removed by ADI, detection limits are ultimately limited by short-lived atmospheric speckles that have a correlation timescale of a few tens of ms, shorter than the time interval required to obtain sufficient FOV rotation to build the ADI reference PSF.

The additional noise attenuation resulting from the combination of n derotated residual images is a function of the correlation of those images. This attenuation is given by $n_{\rm eff}^{1/2}$, where $n_{\rm eff}$ is the effective number of uncorrelated residual images; if all residuals are uncorrelated, then $n_{\rm eff} = n$. Equivalently, for an image sequence of total time $t = t_{\exp} n$, one has to wait for a time

$$\tau_{\rm dcorr} = \frac{n}{n_{\rm eff}} t_{\exp} \tag{2}$$

before two derotated residual images are decorrelated. Thus, the total noise attenuation $N/\Delta N$ is

$$\frac{N}{\Delta N}(t, \theta, \tau, t_{\exp}) \cong \sqrt{\frac{t}{\tau_{\rm dcorr}}} \left[\frac{N}{\Delta N}\right]_S (\theta, \tau, t_{\exp}). \tag{3}$$

TABLE 1
OBSERVATIONS

Object	Date	Nb Images	Field Rotation (degree)	R_{min} (arcsec)	τ_{min} at Meridian and 1″ (minutes)	Strehl Ratio
Vega.....	2004 Aug 26	225	99	0.15	8	0.24[a]
Vega.....	2004 Sep 01	177	69	0.1	8	0.12
HD 18803	2004 Dec 24	90	99	0.15	2	0.10
HD 97334B.....	2005 Apr 18	90	54	0.3	6	0.16

[a] Short exposures for the August 26 run are saturated. Since the September 1 short exposures fill 55% of the pixel electron well at the PSF peak intensity, it is approximated that the Strehl ratio for August 26 is at least 2 times higher than the one estimated for September 1.

For simplicity, let us consider a dominant speckle noise having a correlation timescale τ_{speck}. The ADI noise attenuation resulting from the combination of all difference images is function of τ_{speck}. Its behavior can be defined for two limiting regimes, (1) when either τ_{speck} is much longer than τ or shorter than t_{exp} and (2) τ_{speck} is longer than t_{exp} but shorter than τ.

In the first regime, the residuals of consecutive image differences are decorrelated, either because the correlated structure of the PSF, which lasts for long times ($\tau_{speck} \gg \tau$), has been removed, leaving only Poisson noise ($\tau_{dcorr} = t_{exp}$), or because the PSF structure was already uncorrelated between consecutive images in the first place ($\tau_{speck} \leq t_{exp} \Rightarrow \tau_{dcorr} = t_{exp}$). In this case, the speckle attenuation increases with the square root of the total number of image differences. The decorrelation timescale is simply

$$\tau_{dcorr} = t_{exp}. \quad (4)$$

In the second regime, since τ_{speck} is longer than t_{exp} but shorter than τ, the residuals of consecutive differences are partially correlated and do not average out as efficiently. Assuming that only the noise having a spatial scale $\sim$1 PSF FWHM limits point-source detection, the time needed to decorrelate this noise is the shortest time between τ_{FWHM}, the time for a 1 FWHM FOV rotation, and τ_{speck}. The decorrelation timescale is thus

$$\tau_{dcorr} \cong \min(\tau_{FWHM}, \tau_{speck}). \quad (5)$$

We note that if τ is several minutes and if individual ADI differences are dominated by random short-lived speckles, then the noise attenuation can follow equation (4) for several images but ultimately converges to equation (5) when sufficient averaging of short-lived speckles has occurred.

It is important to known that reducing t_{exp} to increase the number of images for a given image sequence of length t would not result in better detection limits. For the first regime, shorter t_{exp} would mean a smaller companion signal-to-noise ratio (S/N) per image; the final S/N would thus be the same (neglecting losses due to overheads). For the second regime, a shorter t_{exp} would yield quasistatic speckles correlated over more consecutive images, also resulting in the same performance.

We emphasize that ADI guarantees a gain in detection with increasing observing time for both regimes. In the worst case, the speckle attenuation efficiency is limited by field rotation. This is an enormous advantage over classical observation, in which the quasistatic aberrations prevent significant gain after a relatively short observing time. An equation similar to equation (5) also applies to classical observations, but in this case there is no τ_{FWHM}, since the field is not rotating. Speckle attenuation is then governed by τ_{speck}, which can be very large, reducing drastically the efficiency of the observations. Section 6.4 presents a comparison of ADI and classical observations.

4. OBSERVATIONS

The ADI technique was first used at the Gemini North telescope using the Altair adaptive optic system (Herriot et al. 1998) and the near-infrared camera NIRI (Hodapp et al. 2000) in queue mode. Observations and detailed results obtained for three stars of our nearby young star survey, Vega, HD 18803, and HD 97334B are presented. Data for two other stars, HIP 18859 and HD 1405, are also be discussed for comparison, since they have been acquired with a different technique. The exposure time was fixed to 30 s, a time short enough to minimize PSF saturation and the off-axis PSF smearing due to the FOV rotation during the exposure and long enough to get a good observing efficiency and to be limited by the sky background rather than by the read noise at wide separations.

For Vega, HD 18803, and HD 97334B, the imaging sequence consisted of the acquisition of a series of saturated images in the off-methane 1.58 μm 6.5% bandwidth filter with the Cassegrain rotator turned off. This filter was chosen to minimize the brightness ratio of the star to that of methanated exoplanets or brown dwarfs. Unsaturated short exposures were acquired before and/or after the saturated sequence to calibrate detection limits.

For Vega, data were obtained on 2004 August 26 and 2004 September 1 (program GN-2004A-Q-11). In total, 225 and 177 30 s exposures were acquired on August 26 and September 1, respectively. Because of Vega's brightness, short-exposure PSFs of a nearby reference star were acquired for photometric calibration. Seeing conditions were excellent on August 26 and average on September 1. Images were saturated inside a $\sim$6″ diameter. For HD 18803, 90 30 s exposures were obtained on 2004 December 24 (program GN-2004B-Q4), and for HD 97334B, 90 30 s exposures were acquired on 2005 April 18 (program GN-2005A-Q16). For HD 18803 and HD 97334B, seeing conditions were average to good and PSFs were saturated inside diameters of 0.″7. Table 1 summarizes the observations. Strehl ratios were obtained by analyzing unsaturated data acquired before and after each sequence and by comparing the PSF peak intensity with that of a simulated unaberrated PSF having the same pixel sampling, bandpass, and integrated flux. It can be deduced from Table 1 that since R_{min} is less than the saturated radius for all three targets, ADI can be applied at all separations to detect point sources.

As part of Altair science verification, we have obtained a sequence of observations of the star HIP 18859 on 2003 November 18 (program GN-2003B-SV-102). During this sequence, the filter was switched from the broadband H filter to a narrowband filter every fourth exposure to acquire unsaturated images. This data set is discussed in § 6.1.

TABLE 2
ADI Data Reduction Algorithm

Step	Task	Subtask
Reduction	Flat field normalization	
	Bad pixel correction	
	Distortion correction	
	Copy in bigger blank image	
Processing	Image registration	
	Radial profile subtraction	
	Diffraction spikes & saturation masking	
ADI	Subtraction of the median of all images	
	For each 0.6″ wide annulus	Find 4 images with $\tau \geq 1.5\tau_{\min}$
		Median combine these 4 images
		Flux normalization
		Subtract reference annulus
	Calculate parallactic angle	
	Rotate images	
Co-addition.....	Median combination of all differences	
	(optional) Convolution by Gaussian	

Observations of the star HD 1405 were obtained on 2004 August 23 (program GN-2004B-Q-14) with the instrument rotator operating to keep the FOV orientation fixed throughout the sequence. In total, 38 30 s exposures were obtained. These observations are used in § 6.4 for a comparison between ADI and classical observations.

5. ADI DATA REDUCTION ALGORITHM

5.1. *Preliminary Data Reduction*

The data reduction consists of flat-field normalization, bad-pixel correction using a median over surrounding pixels, and distortion correction using software provided by the Gemini staff (C. A. Trujillo 2005, private communication) and modified to use the IDL *interpolate* function with cubic interpolation. Images were then copied into larger blank images to ensure that no FOV was lost when shifting and rotating images. The center of the PSF of the first image of the sequence was then registered to the image center by minimizing the diffraction spikes residuals after subtraction of a 180° rotation of the image. The rest of the images were then registered by cross-correlation of the diffraction spikes with the first image. An azimuthally symmetric intensity profile was finally subtracted from each image to remove the smooth seeing halo.

5.2. *ADI Algorithm*

As discussed in § 3, two methods can be used to subtract the quasistatic PSF structure, subtracting the median of all images or subtracting a reference PSF obtained from a few images acquired as close in time as possible. These two methods can be combined into a single algorithm that optimizes speckle subtraction and minimizes pixel-to-pixel noise. First, the median of all the images is subtracted from each individual image. For a sequence

$$I_1(t_1, \theta_1),\ I_2(t_2, \theta_2),\ I_3(t_3, \theta_3), \ldots,\ I_n(t_n, \theta_n) \tag{6}$$

of n reduced and registered images (see § 5.1), where t_i is the mean time of exposure i, and θ_i is the FOV orientation at time t_i; the first reference subtraction is simply

$$I_i^D = I_i - \text{median}(I_1,\ I_2,\ I_3,\ \ldots,\ I_n). \tag{7}$$

An optimized reference PSF (second method) is then obtained for each image by median combining four images (two acquired before and two after) that show at least a 1.5 FWHM (1 FWHM in the off-methane 6.5% filter is equal to ~3 pixels) FOV orientation difference. This choice ensures that the average τ of the reference PSF is ~0 and that the linear time evolution of quasistatic speckles having $\tau_{\text{speck}} \geq 2\tau$ is removed. For the construction of this reference PSF, the image is broken into many annuli to accommodate for the dependence of $\tau_{\min}$ on the separation. The intensity of the reference PSF is then scaled appropriately inside each annulus to minimize the noise after subtraction. The scaling factor converges to zero if the annulus is dominated by pixel-to-pixel noise or to unity if it is dominated by correlated speckles. The optimized reference PSF is then subtracted. This step can be summarized by the following equation for each annulus i,

$$I_i^{\text{ADI}} = I_i^D - a \times \text{median}(I_{i-b}^D,\ I_{i-b-1}^D,\ I_{i+c}^D,\ I_{i+c+1}^D), \tag{8}$$

where a is a normalizing factor to minimize the noise inside the annulus, and the number of images required to get at least a 1.5 FHWM FOV orientation difference between I_i and the images acquired before and after I_i are b and c, respectively. Differences are then rotated to align the FOV to that of the first image. Finally, a median is taken over all differences. The final combination step is thus

$$I_F^{\text{ADI}} = \text{median}\Big[\mathrm{I}_1^{\text{ADI}},\ \text{rot}\big(\mathrm{I}_2^{\text{ADI}}, \Delta\theta_{1-2}\big),\ \text{rot}\big(\mathrm{I}_3^{\text{ADI}}, \Delta\theta_{1-3}\big),\ \ldots,\ \text{rot}\big(I_n^{\text{ADI}}, \Delta\theta_{1-n}\big)\Big]. \tag{9}$$

Optionally, the final residual image may be convolved by a Gaussian of FWHM equal to that of the PSF to attenuate further the high-frequency noise. Table 2 summarizes the entire ADI reduction algorithm.

6. RESULTS

6.1. *PSF Evolution Timescale*

The PSF noise evolution timescale can be studied through the evolution of the noise attenuation $[N/\Delta N]$ for the difference of

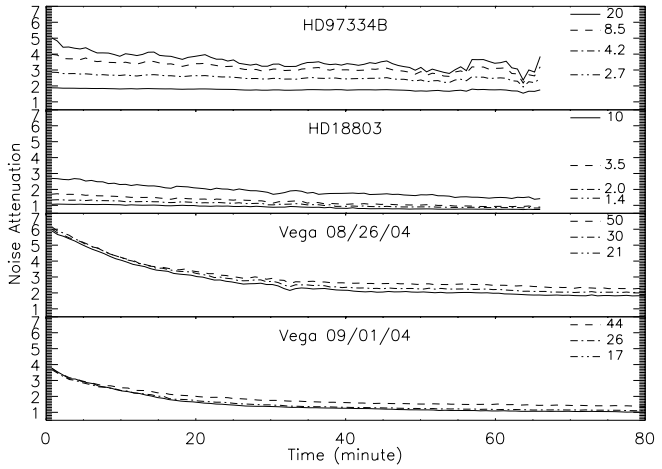

FIG. 2.—Noise attenuation obtained by subtracting images two by two with increasing time interval for HD 97334B, HD 18803, and Vega acquired on 2004 August 26 and on 2004 September 01. Solid, dashed, dot-dashed, and double dot-dashed lines are for 2″, 4″, 6″, and 8″, respectively. For Vega, there is no solid line for 2″, since images are saturated at that separation. Small lines show the estimated noise attenuation limit imposed by photon, sky, flat, read, and dark noises.

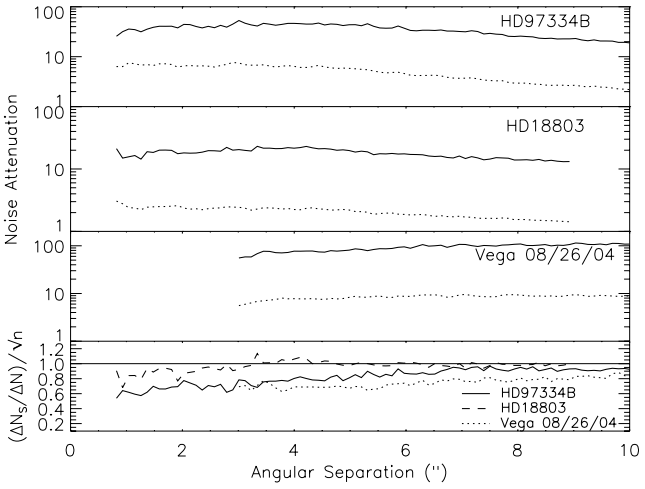

FIG. 3.—Single ADI difference $[N/\Delta N]_S$ and total ADI $[N/\Delta N]$ noise attenuations with separation for HD 97334B, HD 18803, and Vega. Dotted lines show attenuation from a single ADI difference, while solid lines show the attenuation after median combining all ADI differences. The bottom panel shows the ratio of the speckle noise attenuation of the combined ADI difference $[N/\Delta N]$ over that of a single ADI difference $[N/\Delta N]_S$ normalized by the square root of the total number n of images in each sequence. Data for HD 18803 are truncated at 9″ due to a PSF decenter that brought a part of the field >9″ outside the FOV.

two images as a function of the time interval τ. The noise attenuation is the ratio of N to ΔN, which are the measured rms noises in an annulus of width equal to 1 PSF FWHM in the original and in the difference images, respectively. For this analysis, all images have first been unsharp-masked using an 8×8 FWHM box to remove low-frequency noise and then median filtered with a 1×1 FWHM box to remove hot and/or bad pixels. This step is necessary to prevent biasing the noise estimate N of single images and leaves only speckles that have a spatial scale of the order of 1 FWHM. Images were subtracted two by two with increasing time interval. Figure 2 shows the noise attenuation for Vega, HD 18803, and HD 97334B for angular separations of 2″, 4″, 6″, and 8″.

All noise attenuation curves show stronger noise attenuation for shorter time intervals. For HD 18803 and HD 97334B, the noise attenuation reaches ~2–5 inside 4″ for $\tau \sim 2$ minutes. At larger separation, the residuals are limited by pixel-to-pixel noise. For separations less than 4″, the noise attenuation drops by a factor 2 after approximately 60 minutes. For Vega, the noise attenuation reaches ~4–6 at all separations for $\tau \sim 1$ minute and drops by a factor 2 after approximately 15–20 minutes. The stronger noise attenuation achieved on Vega and HD 97334B for short time intervals could be explained by better seeing that stabilizes the structure and enables a better subtraction. In addition, since $\tau_{\rm min}$ is less than 10 minutes at 1″ within $\pm 1^{\rm h}$ from the meridian for all targets having a declination of $-30°$ to $+65°$ at Mauna Kea (see Fig. 1), ADI can be used with little loss of speckle attenuation (~30%) on most of the available sky for separations greater than ~0.″5.

Analysis of the HIP 18859 data set that included a frequent filter change to acquire unsaturated images shows that a drop by a factor of 2 in speckle attenuation occurs following each filter change. This evolution of the PSF structure is probably due to the filter wheel not returning to its exact position after each change. This suggests that the best observing procedure is to prevent any alteration of the optical setup during an observing sequence to maximize the PSF noise stability.

6.2. *ADI Speckle Attenuation*

Figure 3 shows for all ADI targets the average noise attenuations $[N/\Delta N]_S$ achieved for one image difference and the noise attenuation $[N/\Delta N]$ obtained after median combining all the image differences. Again, an 8×8 FWHM unsharp-mask and a 1×1 FWHM median filter were applied to each image to produce this figure. Each ADI difference attenuates by a factor 2–10 the quasistatic speckle noise. Note that these attenuations are better than what is observed in Figure 2, since here the optimized reference PSF is the result of a median of four images, two acquired before and two after. Random speckles are averaged, and the linear speckle evolution with time of speckles having at least $\tau_{\rm speck} \geq 2\tau_{\rm min}$ is removed. As was observed in Figure 2, better seeing conditions (HD 97334B compared to HD 18803) seem to be related to better speckle noise attenuation. A total noise attenuation of ~35 between 0.″8 and 10″ was obtained for HD 18803 and HD 97334B, while this attenuation reached 100 for Vega (August 26 data). The higher attenuation for Vega comes partly from the larger number of images (225 vs. 90) and partly from better seeing conditions, which provided a better attenuation from single image subtractions. HD 97334B and HD 18803 noise attenuations are shown to improve at all separations down to the detector saturation limit and clearly below it, if we extrapolate the performances shown at 0.″8.

The bottom panel of Figure 3 is generated by dividing the ratio of the noise attenuation of the combined ADI difference $[N/\Delta N]$ over the noise of a single ADI difference $[N/\Delta N]_S$ by the expected noise attenuation $n^{1/2}$, if the noise were decorrelated. From equation (3),

$$R = \sqrt{\frac{t_{\rm exp}}{\tau_{\rm dcorr}}}. \tag{10}$$

Because the pixels affected by the secondary mirror support diffraction spikes are masked from the images, the effective number of images combined is reduced at some separations. The bottom panel of Figure 3 has been corrected for this effect, which can reach 20% at small separations. For separations greater than 2″, all three targets achieve more than 70% of the $n^{1/2}$ attenuation expected if residuals are decorrelated. At smaller separations the attenuation is lower, revealing a correlated noise in successive

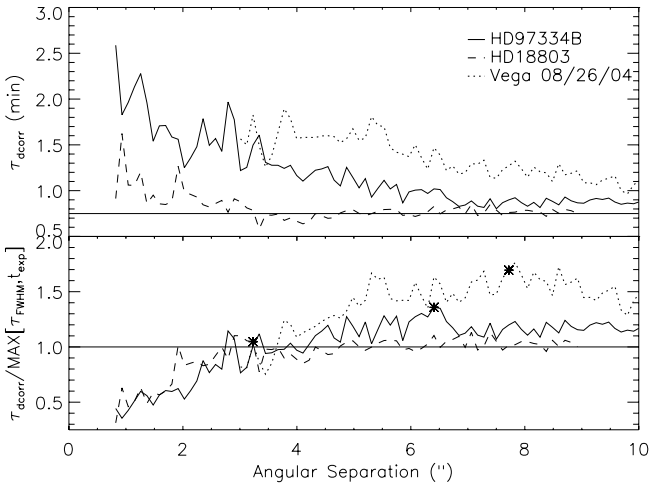

FIG. 4.—*Top panel*: Estimated residual speckle decorrelation timescale τ_{dcorr} as a function of angular separation for HD 97334B, HD 18803, and Vega (August 26). *Bottom panel*: Normalized residual speckle decorrelation time as a function of angular separation for the same three targets. The star symbol on each curve indicates at what separation $\tau_{FWHM} = t_{exp}$.

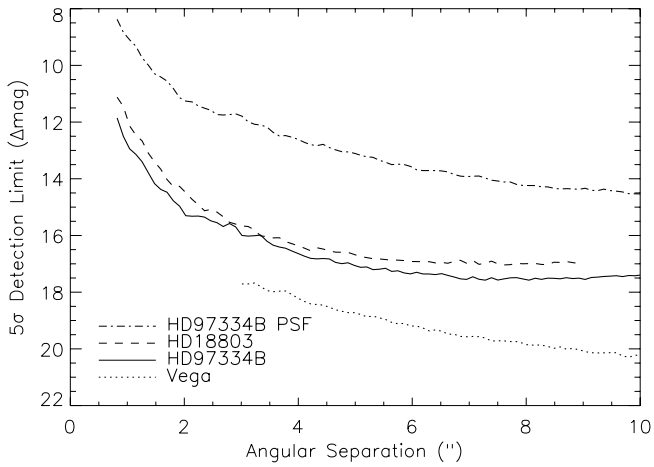

FIG. 5.—Final ADI detection limits (5 σ) as a function of angular separation for HD 18803, HD 97334B, and Vega (August 26). The initial detection limit for the HD 97334B PSF (*dot-dashed line*) is also shown to illustrate the ADI noise attenuation performance.

ADI differences that lowers the number of independent images (see eq. [5]).

Since ADI does not achieve a $n^{1/2}$ noise attenuation gain at all separations, the bottom panel of Figure 3 and equation (10) can be used to estimate the residual speckle decorrelation time that is currently limiting ADI performances. Figure 4 (*top*) shows the estimated decorrelation timescale as a function of angular separation. Typical decorrelation times are of the order 1–3 minutes and are generally smaller at larger angular separations. Normalizing these curves by the time max (τ_{FWHM}, t_{exp}) (see Fig. 4, *bottom*), it can be deduced that for separations less than 3″, since τ_{dcorr} is less than τ_{FWHM}, ADI differences are limited by residual speckles having $\tau_{speck} < \tau_{FWHM}$. These residual speckles evolve faster than the time needed to obtain an ADI reference PSF and cannot be subtracted by ADI. It is tempting to believe that these residual speckles are produced by the telescope active optics system, since it operates on a similar timescale (F. Rigaut 2005, private communication). For HD 97334B and HD 18803, for separations greater than 3″, ADI is limited by the FOV rotation or the noise is decorrelated (limited by t_{exp}). For Vega, the decorrelation time increases until $\tau_{FWHM} = t_{exp}$ and then decreases. The fact that τ_{dcorr} is significantly greater than τ_{FWHM} when $\tau_{FWHM} \geq t_{exp}$ suggests that Vega ADI differences, at those separations, are limited by correlated noises that are bigger than 1 FWHM. This noise thus requires more than a FWHM FOV rotation to be decorrelated. The upper limit at ~1.5 FWHM is expected, since a minimal FOV rotation of 1.5 FWHM (τ_{min}) has been chosen to build the ADI-optimized reference PSF. The ADI-optimized reference PSF subtraction is a temporal filter that guarantees that no noise can have a decorrelation time longer than the time needed for a ~1.5 FWHM FOV rotation.

6.3. *Contrast Performances*

Figure 5 shows detection limits (5 σ) in magnitude difference as a function of angular separation obtained with the ADI technique for all three ADI targets. To produce this figure, data were reduced following the procedure explained in § 5.1. No unsharp mask was used for the ADI reduction, since multiple tests have shown that while this filter is effective for suppressing the low-frequency spatial noise, it does not improve candidate S/N and the photometry is slightly biased in the process. The detection limits are calculated using the ratio of simulated companion peak intensities over the noise in the residual image as a function of angular separation. The flux-normalized unsaturated PSF was then used to simulate smeared companion PSFs as a function of angular separation. The noise is calculated inside annuli of increasing diameter and width equal to 1 PSF FWHM. To account for the PSF smearing effect due to FOV rotation, the image and simulated companions were convolved with elliptical Gaussian of 1 FWHM in the radial direction and 1 FWHM plus a smearing term in the azimuthal direction, the smearing term ranging from 0 at the center to typically 2 FWHM at 10″, depending on the rotation rate of the FOV. Finally, detection limits were corrected for the Altair estimated anisoplanatism following the Strehl *S* equation found in the Gemini web page,[4]

$$S(\theta) = S_0 e^{-(\theta/12.5)^2}, \tag{11}$$

where θ is expressed in arcseconds. The detection limit obtained with the ADI technique on Vega at separations greater than ~5″ is 2 orders of magnitude deeper than the Palomar *H*-band image (Metchev et al. 2003) and approximately a factor of 10 deeper than the Keck *K*-band image of (Macintosh et al. 2003). The current speckle attenuation (20–100) achieved with ADI is comparable or better to what is currently obtained (50) from one *HST* orbit using the roll subtraction technique. Although the ADI technique is inherently optimized for relatively large separations, the good Gemini PSF stability enables excellent performances at subarcsecond separations. Indeed, the ADI contrast of $\Delta m = 11.1-11.9$ (5 σ) at 0.″8 obtained on HD 18803 and HD 97334B equals the $\Delta m = 11.0$ (5 σ) at 0.″8 obtained with the simultaneous differential imaging (SDI) VLT camera optimized for multiwavelength speckle suppression (Biller et al. 2006). This shows the potential of ADI to achieve high-contrast detection at subarcsecond separations using a simple, yet efficient, observing technique with standard instruments. Figure 6 illustrates the noise attenuation obtained for Vega (August 26) using the ADI technique.

[4] See http://www.gemini.edu/sciops/instruments/altair/altairIndex.html.

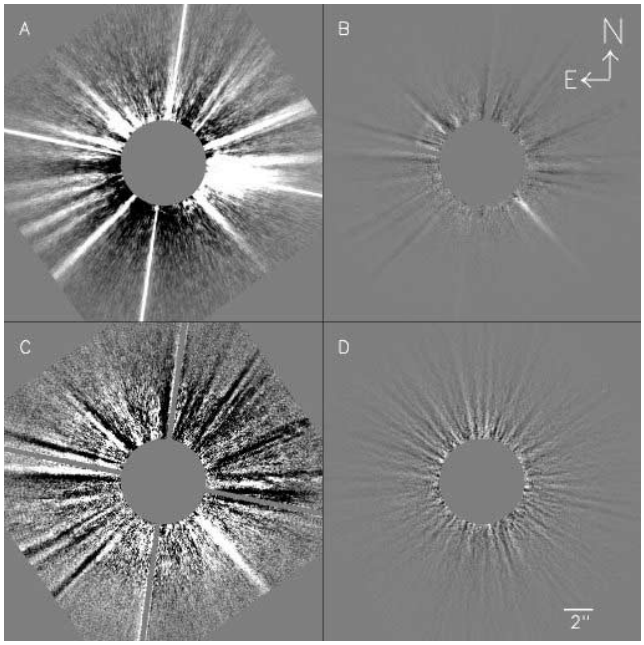

FIG. 6.—Vega (August 26) ADI data reduction. *A*: Single image after flat-field normalization, bad-pixel correction, distortion correction, registering, and removal of an azimuthally symmetric profile. FOV is $22'' \times 22''$ using a linear intensity range of $\pm 10^{-6}$ from the estimated PSF peak intensity. *B*: Single ADI difference image shown with the same intensity range. *C*: Same as B, but with an intensity range 25 times smaller. *D*: Final combination of all ADI differences shown with the same intensity range as C. The central saturated $6''$ diameter region as well as diffraction from the secondary mirror supports have been masked.

Mass limits corresponding to these observations, corrected for the filter use,[5] are estimated using evolutionary models from Baraffe et al. (2003), assuming ages of 350, 45, and 85 Myr for Vega, HD 18803, and HD 97334B, respectively (Song et al. 2001; Montes et al. 2001). Both HD 18803 and HD 97334B achieve detection limits of $1–2M_{\rm Jup}$ at $3''$ (60 AU for both targets), while $\sim 3M_{\rm Jup}$ is obtained for Vega at $8''$ (63 AU). The ADI technique is thus well suited to survey Jovian companions at intermediate separations (50–300 AU) orbiting young nearby stars.

6.4. *Comparison between ADI and Classical Imaging*

In the previous sections it was shown that the ADI technique can achieve high contrast given a sufficiently long integration time and good PSF stability. To compare the performances of ADI and classical observations, we analyze the first 38 images of the HD 97334B ADI sequence and the 38 images of the HD 1405 "classical" sequence. For this analysis, both data sets have been reduced according to § 5.1. Furthermore, an 8×8 FWHM unsharp mask was applied to all images to remove the low spatial frequency quasistatic noise. Then a 1×1 FWHM median filter was applied to all images to remove the bad and/or hot pixels. These steps are performed here only to bring the classical observations on even ground with ADI, in order to study the evolution of the noise at spatial scales that most severely limit point-source detections. For the HD 97334B sequence, image differences were obtained according to § 5.2; these differences were then rotated to align the FOV to that of the first image.

[5] The star-to-planet brightness ratio is reduced by a factor of ~2.6 when using a 6.5% bandpass methane filter instead of a broadband *H*, as derived from a theoretical spectrum of Allard et al. (2001).

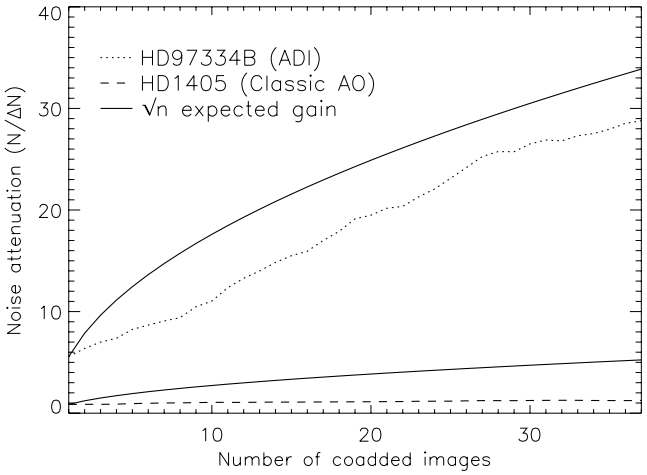

FIG. 7.—Normalized noise attenuation from the median combination of an increasing number of images (differences in the ADI case) at $2''$ separation. Each single image represents 30 s exposure time. The dotted and dashed lines are the ADI reduction and the HD 1405 without field rotation sequence, respectively. See § 6.4 for more details.

An increasing number of images (differences for HD 97334B) of both sequences were median combined to study the noise attenuation as a function of the total observing time at $2''$; the results are presented in Figure 7. The ADI reduction technique achieves 30 times better speckle noise attenuation compared to classical AO observations in 30 minutes integration time. This figure also illustrates the power of ADI imaging, in which noise attenuation, and thus companion S/N, increases nearly as the expected $n^{1/2}$, while it saturates rapidly for normal imaging.

7. DISCUSSION

ADI is a general high-contrast imaging technique that can be applied to any existing or upcoming large altitude/azimuth telescope. It is also flexible enough to be combined with a number of other high-contrast imaging techniques.

ADI at small separations ($<1''$) requires long time intervals and thus may suffer from PSF variations. These variations come from variable seeing and slowly evolving quasistatic aberrations from the telescope and instrument optics. Unsaturated data inside $0''.8$ are required to estimate performances. Extrapolation from our observations predicts that noise attenuation will be limited by speckles evolving faster than $\tau_{\rm FWHM}$ required for a 1 FWHM FOV rotation. Speckle noise attenuation of the order of a factor of 10 should be feasible for 1 hr sequences. The use of a multi-wavelength instrument (Marois et al. 2000, 2004, 2005; Doyon et al. 2004; Lafrenière et al. 2004; Biller et al. 2004) or an Integral Field Unit (IFU; Sparks & Ford 2002) to acquire simultaneous images at multiple wavelengths across the methane absorption band head at 1.6 μm through the simultaneous spectral differential imaging (SSDI) technique (Racine et al. 1999; Marois et al. 2000, 2004, 2005; Biller et al. 2004) could provide good short-lived and common-path speckle attenuations and increase detection limits. It has been shown that SSDI instruments are ultimately limited by non–common-path aberrations, which are expected to be stable over long periods of time, as they come almost entirely from the instrument itself (Marois et al. 2005). Hence, the ADI technique nicely complements SSDI since it can be used to subtract the residuals caused by the non–common-path aberrations.

Future high-contrast instrumentation for 8–10 m class or larger telescopes based on high-order adaptive optics (AO)

systems (Macintosh et al. 2004; Mouillet et al. 2004) will most likely improve the stability of the PSF. Thus, if combined with such instruments, ADI could prove even more successful. These new AO systems will also provide the high Strehl ratios required to bring coronagraphy at the forefront of high-contrast imaging. However, even a very good coronagraph cannot totally suppress the light from uncorrected quasistatic wave front errors, and some level of quasistatic speckle noise will inevitably be present in coronagraphic observations. ADI would be a nice addition to coronagraphy, as it could attenuate those residual speckles.

Ideally, all the techniques mentioned above, ADI, SSDI, high-order AO, and coronagraphy, could be used together to form an extremely powerful tool to detect exoplanets and brown dwarfs around stars.

8. CONCLUSION

The ADI observing technique was described and its performance using Altair NIRI at Gemini presented. It was shown that faint companions can be detected with better S/N than achieved with classical observing techniques for a wide range of declinations. The ADI technique produces a reference PSF from the same target imaging sequence, removing the need to move to a nearby star for PSF calibration or to acquire sky exposures (for *H*-band imaging). Since the reference PSF is built using images acquired minutes apart, the reference PSF shows a good quasistatic speckle correlation.

The stability of the PSF plays a crucial role in ADI, as it not only determines the speckle attenuation from the reference image subtraction, but also determines the regime in which the noise is attenuated with increasing observing time. It was reported that at Gemini with Altair NIRI using 30 s exposures, the PSF evolves on timescales of $\sim$10–60 minutes, and the attenuation by subtraction of a reference image reaches $\sim$2–6 for short time intervals, achieving better speckle attenuation with better seeing conditions. The observations of HIP 18859, for which a filter change during the sequence reduced significantly the speckle attenuation, underscore the importance of maintaining the optical setup fixed during the sequence. It was shown that the gain in S/N with increasing total observing time for separation greater than $2''$ reaches more than 70% of the optimal case, indicating that the noise is mostly decorrelated between residual images for these separations. Typical residual speckle decorrelation time is of the order of a few minutes, possibly coming from the telescope active optics system. The speckle noise residuals decorrelate faster for objects having faster FOV rotation. In all cases, ADI guarantees a larger gain with longer observation sequences. To our knowledge, this is the first time that such behavior is clearly demonstrated for an acquisition and reduction technique designed for speckle attenuation. The wall raised by quasistatic speckles that prevents a gain with longer integration time for standard observing techniques (Marois et al. 2003, 2005; Masciadri et al. 2005) can thus be removed by ADI. Comparison with a classical imaging technique shows that ADI achieves 30 times better speckle attenuation in 30 minutes integration time.

The noise attenuation obtained on Vega was 100, reaching a contrast of $\sim$20 mag at $8''$ separation (63 AU). Observations of the young stars HD 18803 and HD 97334B yielded detection limits in difference of magnitude of 11.1–11.9 at $0''.8$, similar to the SDI camera at VLT (Δm of $\sim$11 at $0''.8$), which is an optimized speckle suppression instrument. When combined with substellar models and estimated ages for these stars, these observations show that ADI is well suited to search for Jovian companions having a mass greater than $1–2M_{\rm Jup}$ 50–300 AU away from nearby young stars. Finally, ADI could easily and advantageously be combined with SSDI, high-order AO, and coronagraphy to improve the detection limits of exoplanets and brown dwarfs at all separations.

This research has made use of the SIMBAD database, operated at CDS, Strasbourg, France. Authors would like to thank René Racine for his comments on the manuscript, François Rigaut and the Gemini observing staff for introducing a neutral density filter inside Altair that made Vega observations possible, and Michael Fitzgerald, Paul Kalas, James Graham, Mike Liu, Rémi Soummer, and Étienne Artigau for discussions about data reduction techniques and/or speckle statistics. The authors wish to recognize and acknowledge the very significant cultural role and reverence that the summit of Mauna Kea has always had within the indigenous Hawaiian community. We are most fortunate to have the opportunity to conduct observations from this mountain. This work is supported in part through grants from the Natural Sciences and Engineering Research Council, Canada and from the Fonds Québécois de la Recherche sur la Nature et les Technologies, Québec. This research was also partially performed under the auspices of the US Department of Energy by the University of California, Lawrence Livermore National Laboratory under contract W-7405-ENG-48, and also supported in part by the National Science Foundation Science and Technology Center for Adaptive Optics, managed by the University of California at Santa Cruz under cooperative agreement AST 98-76783.

REFERENCES

Allard, F., Hauschildt, P. H., Alexander, D. R., Tamanai, A., & Schweitzer, A. 2001, ApJ, 556, 357

Baraffe, I., Chabrier, G., Barman, T. S., Allard, F., & Hauschildt, P. H. 2003, A&A, 402, 701

Biller, B. A., Close, L.,Lenzen, R., Brandner, W., McCarthy, D., Nielsen, E., & Hartung, M. 2004, in SPIE Proc. 5490, Advancements in Adaptive Optics, ed. D. B. Calia, B. L. Ellerbroek, & R. Ragazzoni (Bellingham: SPIE), 389

Biller, B. A., et al. 2006, in IAUC Proc. 200, in press

Doyon, R., Lafrenière, D., Marois, C., Racine, R., & Nadeau, D. 2004, in SPIE Proc. 5382, Emerging Optoelectronic Applications, ed. G. E. Jabbour & J. T. Rantala (Bellingham: SPIE), 21

Fraquelli, D. A., Schultz, A. B., Bushouse, H., Hart, H. M., & Vener, P. 2004, PASP, 116, 55

Herriot, G., Morris, S., Roberts, S., Fletcher, J. M., Saddlemyer, L. K., Singh, G., Véran, J., & Richardson, E. H. 1998, in SPIE Proc. 3353, Adaptive Optical System Technologies, ed. D. Bonaccini & R. K. Tyson (Bellingham: SPIE), 488

Hodapp, K., Hora, J., Graves, E., Irwin, E. M., Yamada, H., Douglass, J. W., Young, T. T., & Robertson, L. 2000, in SPIE Proc. 4008, Optical and IR Telescope Instrumentation and Detectors, ed. M. Iye & A. F. Moorwood (Bellingham: SPIE), 1334

Lafrenière, D., Doyon, R., Racine, R., Marois, C., & Nadeau, D. 2004, in SPIE Proc. 5492, Ground-Based Instrumentation for Astronomy, ed. A. F. M. Moorwood & I. Masanori (Bellingham: SPIE), 500

Liu, M. C. 2004, Science, 305, 1442

Macintosh, B. A., Becklin, E. E., Kaisler, D, Konopacky, Q., & Zuckerman, B. 2003, ApJ, 594, 538

Macintosh, B. A., et al. 2004, in SPIE Proc. 5490, Advancements in Adaptive Optics, ed. D. B. Calia, B. L. Ellerbroek, & R. Ragazzoni (Bellingham: SPIE), 359

Marois, C. 2004, Ph.D. thesis, Univ. de Montréal

Marois, C., Doyon, R., Racine, R. & Nadeau, D. 2000, PASP, 112, 91

———. 2003, in EAS Pub. Ser. 8, Astronomy with High Contrast Imaging, ed. C. Aime & S. Soummer (Les Ulis: EDP Sciences), 233

Marois, C., Doyon, R., Racine, R., Nadeau, D., Riopel, M., Vallée, P., & Lafrenière, D. 2005, PASP, 117, 745
Marois, C., Racine, R., Doyon, R., Lafrenière, D., & Nadeau, D. 2004, ApJ, 615, L61
Masciadri, E., Mundt, R., Henning, T., Alvarez, C., & Barrado y Navascués, D. 2005, ApJ, 625, 1004
McLean, I. S. 1997, Electronic Imaging in Astronomy: Detectors and Instrumentation (Chichester: Wiley)
Metchev, S. A, Hillenbrand, L. A., & White, R. J. 2003, ApJ, 582, 1102
Montes, D., López-Santiago, J., Gálvez, M. C., Fernández-Figueroa, M. J., De Castro, E., & Cornide, M. 2001, MNRAS, 328, 45
Mouillet, D., Lagrange, A. M., Beuzit, J.-L., Moutou, C., Saisse, M., Ferrari, M., Fusco, T., & Boccaletti, A. 2004, in ASP Conf. Ser. 321, High Contrast Imaging from the Ground, ed. J.-P. Beaulieu, A. Lecavelier des Etangs, & C. Terquem (San Fransisco: ASP), 39
Racine, R., Walker, G. A. H., Nadeau, D., Doyon, R., & Marois, C. 1999, PASP, 111, 587
Schneider, G., & Silverstone, M. D. 2003, SPIE Proc. 4860, High-Contrast Imaging for Exo-Planet Detection, ed. A. B. Schultz (Bellingham: SPIE), 1
Song, I., Caillault, J.-P., & Barrado y Navascués, D., Stauffer, J. R. 2001, ApJ, 546, 352
Sparks, W. B., & Ford, H. C. 2002, ApJ, 578, 543